Polymer Bulletin (2023) 80:11317–11327
https://doi.org/10.1007/s00289-022-04578-4

ORIGINAL PAPER

Effects of SWCNT content on the electrospinning behavior and structure formation of a PVDF/SWCNT composite web

Jhwan Lim[1,2] · Hansol Park[1,2] · Sejin Choi[1,2] · Han Seong Kim[1,2]

Received: 11 July 2022 / Revised: 28 October 2022 / Accepted: 14 November 2022 / Published online: 1 December 2022

Abstract
In this study, the effect of the addition of conductive materials on the solution properties, electrospinning behavior, and electrospun web structure of polyvinylidene fluoride (PVDF) was investigated. A PVDF/single-walled carbon nanotube (SWCNT) composite was prepared by adding various amounts of SWCNT to a PVDF solution, and a PVDF/SWCNT web was produced by electrospinning. To fabricate a polymer solution complex with a conductive material, it is important to understand the change in electrospinning behavior according to the properties of the solution. The properties of the composite solution were analyzed with respect to the SWCNT ratio in the solution, and the real-time effects on electrospinning behavior were compared and analyzed. The electrospinning behavior considerably differed depending on the properties of the solution. In this study, SWCNT was added in the range of 0–0.02%, and as the SWCNT content increased, the collection area decreased by 25%, the fiber diameter increased from 1.69 ± 0.88 to 1.83 ± 1.22 μm, and the PVDF fiber β-phase content reduced by approximately 6%. The PVFD/SWCN spinning behavior difference analysis and structure formation change according to the SWCNT ratio are useful for controlling the diameter, collection area, and crystallinity in the fiber process of PVDF. They are also expected to be useful for controlling the electrospinning behavior and fiber formation of various polymer materials based on the addition of conductive materials.

Keywords Electrospinning · Electrospun fiber · Dynamic behavior · Polyvinylidene fluoride · Single-walled carbon nanotube · Fiber formation

✉ Han Seong Kim
hanseongkim@pusan.ac.kr

[1] School of Chemical Engineering, Pusan National University, 2, Busandaehak-ro 63boen-gil, Geumjeong-gu, Busan 46241, Republic of Korea

[2] Institute of Advanced Organic Materials, Pusan National University, 2, Busandaehak-ro 63boen-gil, Geumjeong-gu, Busan 46241, Republic of Korea

Introduction

Polyvinylidene fluoride (PVDF) is a polymer with excellent chemical and heat resistance, durability, and flexibility [1–3]. PVDF has a variety of crystal structures comprising α, β, and γ phases and has been applied in many applications, such as sensors, filters, and secondary battery separators [4–12]. In particular, it is a polymer piezoelectric material that has been used as a substitute for ceramic piezoelectric materials and has attracted considerable attention as a wearable material because of its high flexibility [13–15]. Material compositions such as polymer–nanoparticle composites are opening new possibilities in various fields. [16]. Nanomaterials play a crucial role in the manufacture of polymer nanocomposites owing to their unique physical and chemical properties, which change according to their characteristics, size, and content. Polymer nanocomposites have gained theoretical and practical interests, and offer practical applications because of their appealing properties, such as high durability, processability, and functionality, not only in the product but also in the process [17–20]. Methods for producing polymer fibers include phase separation, freeze-drying, interfacial polymerization, and electrospinning. Among them, electrospinning is used in various fields owing to its ease of use and because it allows for easy nanofiberization of various polymers [21]. To use PVDF in piezoelectric devices, the formation of a β-phase crystal structure is essential. The β-phase crystal structure of PVDF is easily induced by elongating the fiber and applying an electric field during electrospinning [22–24]. Many studies have, therefore, been conducted on the effects of various additives on the efficiency of PVDF in the fabrication of piezoelectric sensors and generators [25–27]. Electrospinning is a convenient method for fabricating nanofiber membranes or webs containing organic and inorganic components using polymer melts or solutions [28, 29]. It is based on the principle that a strong electric field and strong repulsive forces between polymer drops that have been electrically charged using a high-voltage power source will result in the generation of fibers. Despite the simplicity of this principle, its detailed mechanism is complex. Therefore, it is necessary to understand the factors affecting electrospinning so that a stable electrospinning setup can be established and fiber formation can be controlled [30, 31]. In this study, solution properties, including surface tension, viscosity, and solution conductivity, of composite solutions containing single-walled carbon nanotubes (SWCNT), an agent that can improve the piezoelectric performance of PVDF, were investigated. The effects of these properties on the electrospinning behavior resulting from the addition of different amounts of SCWNT to a PVDF solution were analyzed and compared. In addition, by analyzing the real-time dynamic behavior during the electrospinning process, changes in the drop and jet behavior with the solution properties and their effects on the formed fiber and web structures were elucidated.

Experimental

Materials

PVDF powder (M_w = 534,000; Sigma-Aldrich Inc., USA) and SWCNT (US Research Nanomaterials, Inc.) were added to a solvent mixture of *N,N*-dimethylformamide (DMF, Junsei Chemical Co. Ltd., Japan) and acetone (Duksan Pure Chemicals Co. Ltd., Republic of Korea). After preparing a 14 wt% PVDF solution and dispersions of 0, 0.01, 0.02, 0.03, and 0.04 wt% SWCNT with the same weight, each prepared solution and dispersion was mixed with additional PVDF powder to obtain 15 wt% PVDF solutions with 0, 0.005, 0.01, 0.015, and 0.02 wt% SWCNT.

Fabrication of PVDF/SWCNT webs

The PVDF/SWCNT webs were fabricated via electrospinning. The PVDF/SWCNT solution was fed through a 21 G metal nozzle (inner diameter = 0.495 mm) at 20 kPa using an air compressor to maintain a constant feeding rate. The solution and nozzle were applied at a high voltage of 9.5 kV. The tip-to-collector distance (TCD) was 15 cm. The resulting PVDF/SWCNT web was collected for 300 s at room temperature (20 °C) and a relative humidity of 50% and subsequently dried for 24 h.

Characterization

To analyze the properties of the solutions, the surface tension, shear viscosity, and conductivity of each PVDF/SWCNT solution were measured. These measurements were performed using a surface tension meter (SEO-DST30M, SEO Ltd, Suwon, Korea), viscometer (DV-II + Pro, AMETEK Brookfield Inc., MA, USA), and conductivity meter (HI 8633, HANNA Instruments Inc., Rhode Island, USA). Images of the drop ejected from the nozzle tip and the jet from the drop to the collector were captured using a charge-coupled device (CCD) camera (SCC-B2315, Samsung Electronics Co., Suwon, Republic of Korea) over the entire duration of the electrospinning process (Fig. 1). The original drop and jet images were processed as binary images (black and white, respectively) using an optimal threshold and intensity. The changes in the drop and jet areas with spinning time were analyzed using a self-programmed image analysis tool. The current between the nozzle tip and collector during electrospinning was measured using a precision multimeter (8846A, Fluke Co., Everett, WA, USA). Images of the fabricated PVDF/SWCNT webs were captured using a scanner (PIXMA E510, Canon Inc., Tokyo, Japan) and converted to binary contour images to analyze the distribution of the deposited webs. The morphologies of the PVDF/SWCNT webs were observed using field-emission scanning electron microscopy (FE-SEM; SUPRA25, Carl Zeiss Co. Ltd., Oberkochen, Germany). The β- and α-phase compositions of PVDF were measured and analyzed using a Fourier

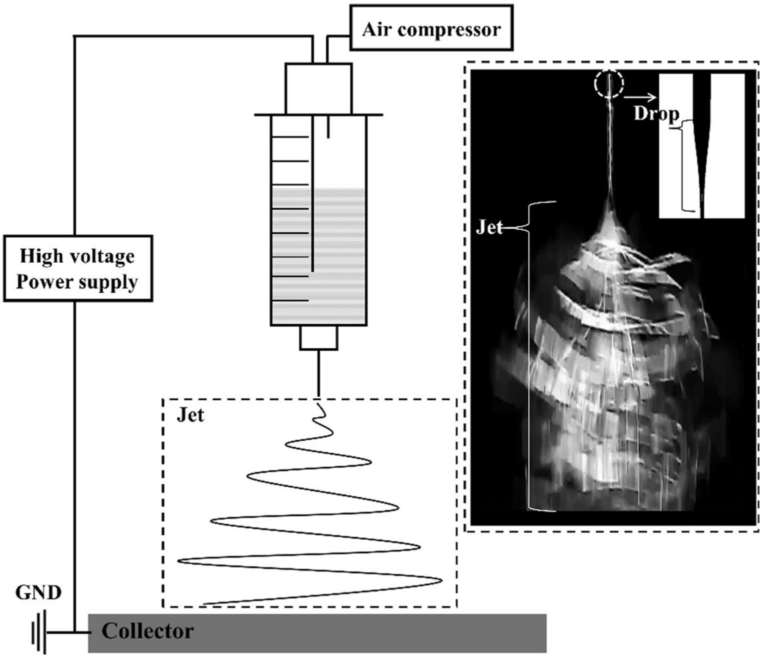

Fig. 1 Schematic of electrospinning setup and image of drop and jet captured by the CCD camera during electrospinning

transform infrared (FT-IR) spectrophotometer (IRAffinity-1, Shimadzu Co. Ltd., Kyoto, Japan).

Results and discussion

Solution properties, including the surface tension, viscosity, and conductivity, significantly influence the spinning dynamic behavior during the electrospinning process. Figure 2 shows the surface tension, viscosity, and conductivity of solutions containing different ratios of SWCNT. The numerical values of all three solution properties

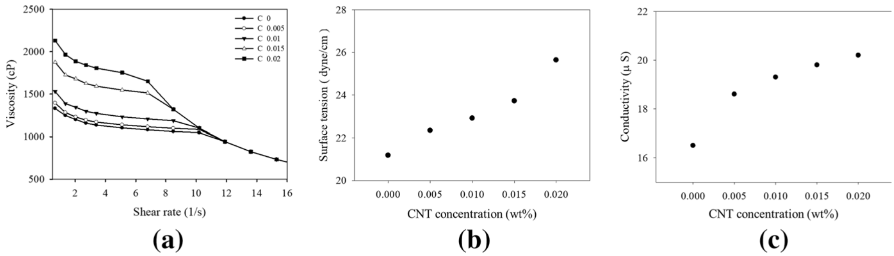

Fig. 2 Characteristics of PVDF/SWCNT solutions: **a** shear viscosity, **b** surface tension, and **c** solution conductivity

tended to increase with the SWCNT content. Figure 2a shows that the addition of SWCNT led to an increase in shear viscosity. This increase is attributed to the PVDF acting as a phase stabilizer for the stable dispersion of SWCNT in the solution through its interaction with SWCNT, which increased the entanglement of the polymer. Although the solution contains a small amount of SWCNT, even if PVDF is present as a phase stabilizer, it is thought that the strong cohesive force between the SWCNTs increases the shear viscosity of the solution. Similarly, the increase in surface tension due to the addition of SWCNT, as shown in Fig. 2b, is attributed to the increased interaction between the PVDF polymer chain and SWCNT. The conductivity increase shown in Fig. 2c is attributed to an increase in the charge mobility of the solution with the addition of SWCNT, which is a conductive material.

In the first step of the electrospinning process, the instability of the droplets attached to the nozzle tip was investigated. The change in the drop area, which represents the number of droplets, was determined by both the jet velocity induced by the applied voltage and the surface tension and velocity of the solution ejected from the nozzle. As shown in Fig. 3, a more significant fluctuation occurred in the drop area change when SWCNT was not added than when SWCNT was added, and the drop area decreased as the SWCNT content increased. These results are attributed to the decrease in the amount of solution ejected from the nozzle at a fixed feeding rate and applied voltage, owing to the increase in shear viscosity and surface tension with increasing SWCNT content, as shown in Fig. 2. In addition, it is considered that the charge repulsion force weakened owing to the increase in solution conductivity, which also contributes significantly during electrospinning.

The electrospinning jet area represents the amount of solution ejected from a drop. In addition, the dynamic behavior of the jet is an important electrospinning factor that affects fiber and web formation. Figure 4 shows the results of an analysis of the real-time jet behavior images, jet area change, and current between the nozzle and collector according to the SWCNT content. As shown in Fig. 4a,

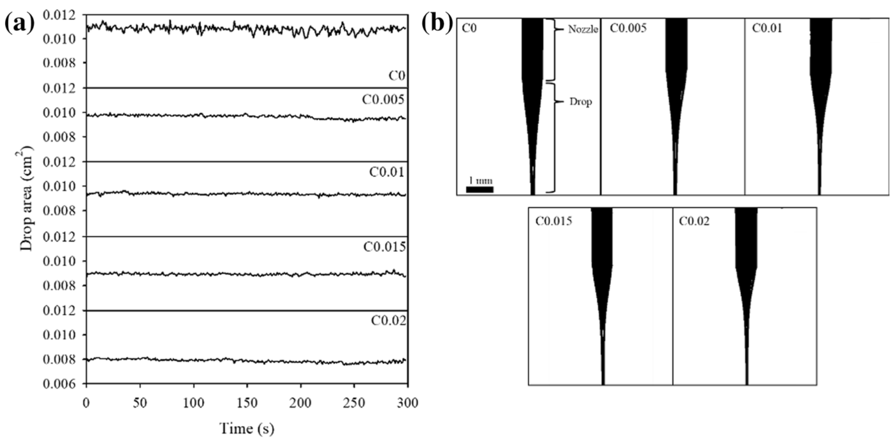

Fig. 3 **a** Change in drop area over 300 s of the electrospinning process. **b** CCD images of the drop area at various concentrations of SWCNT

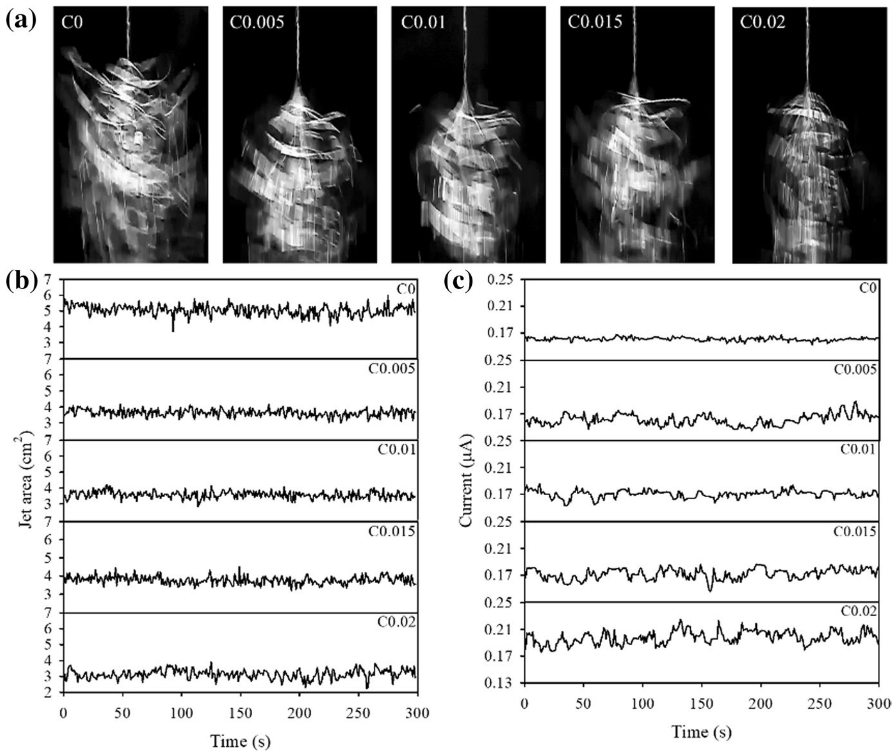

Fig. 4 **a** CCD images of jet areas with various SWCNT concentrations. **b** Change in jet area during the electrospinning process over 300 s. **c** Change in current during the electrospinning process at various solution concentrations

b, the jet area tends to decrease as the SWCNT content increases. This increase can be attributed to the following two factors: First, the increase in the surface tension and shear viscosity of the solution and ejected droplets with the SWCNT content, as shown in Fig. 3, led to a decrease in the amount of jet ejected from the droplets owing to the applied voltage; secondly, by analyzing the change in current during the electrospinning process shown in Fig. 4c, it can be seen that the change became more unstable with the addition of more SWCNT, and the overall current increased. As the SWCNT content increased, the amount of current flowing through the jet increased during electrospinning of the solution droplets electrically charged by the applied voltage. The reduction in the overall area of the jet was attributed to the reduction in the charge repulsion as the current increased.

A contour analysis was performed on the PVDF/SWCNT webs fabricated via electrospinning, as shown in Fig. 5. The binary image-scale light intensities of the web images were analyzed by filtering the intensities from 40 to 255 in 22 steps to evaluate the distribution of the formed fibers. In Fig. 5b, the filtered area with an intensity of 50 is the largest in the web without SWCNT and smallest in the web with the highest SWCNT content of 0.02 wt%. These results are corroborated by

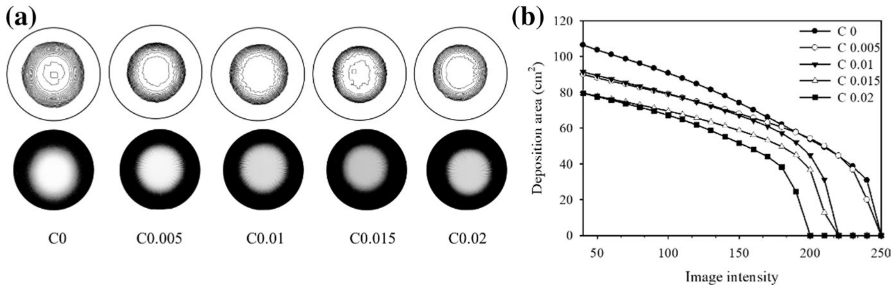

Fig. 5 **a** Threshold processing images of PVDF/SWCNT web deposition and actual images and **b** corresponding contour analysis of webs

the actual images shown in Fig. 5a and are attributed to the reduced jet area and bending radius at higher SWCNT content, as shown in Fig. 4. The web with 0.02 wt% SWCNT exhibited no area in which the intensity reached or exceeded 200. The higher the SWCNT content, the lower the deposition area of the web. This is because the fibers were more densely formed at higher SWCNT contents owing to the reduced jet area and radius, and the addition of SWCNT resulted in a darker color in the web, leading to the absence of areas with high intensities.

Figure 6a shows the morphology of the PVDF/SWCNT webs fabricated via electrospinning with different SWCNT contents. All the webs were formed in a stable fibrous form without beads. Figure 6b shows the fiber diameter distribution of the webs fabricated by electrospinning. The average diameters of the webs with SWCNT contents from 0 to 0.02 wt% were 1.69 ± 0.88, 1.73 ± 0.89, 1.78 ± 1.10, 1.8 ± 1.23, and 1.83 ± 1.22 µm, respectively. As the SWCNT content increased, the average fiber diameter increased. This decrease led to an increase in the surface tension and shear viscosity, and an increase in the amount of current in the jet during the electrospinning process. This decrease was followed by an increase in the surface tension and shear viscosity, and an increase in the amount of amperage of the jet during the electrospinning process. In electrospinning, the increasing surface tension and shear viscosity of the solution resist the charge repulsion force in the drop and jet due to the applied high voltage. Accordingly, in the fiber drawing stage of jet whipping during the spinning process, the relatively high surface tension and increased shear viscosity prevented the fiber from drawing, and the average diameter

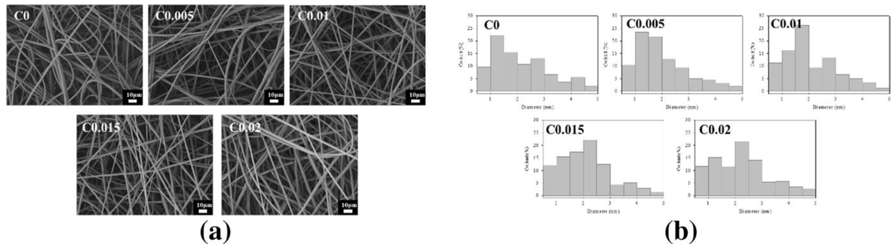

Fig. 6 **a** FE-SEM images of PVDF/SWCNT webs fabricated by electrospinning. **b** Fiber diameter distributions

increased. This was also indicated by the reduced area and bending radius of the jet in the behavior analysis. In addition, because of the increase in solution conductivity due to the addition of SWCNTs, the charges flow to the ground relatively easily owing to the high voltage. As a result, the repulsive force is relatively weak owing to the lower charge density of the drop, and jet acts as a stretching force.

Fourier transform infrared spectroscopy (FT-IR) was performed to determine the crystallinity of the fabricated PVDF/SWCNT webs. Representative α-phase peaks appeared in the FT-IR spectra at 612 and 763 cm^{-1} (skeletal bending and CF2 bending), 795 cm^{-1} (CH2 rocking), and 975 cm^{-1} (CH2 twisting). Representative β-phase peaks appeared at 510 and 840 cm^{-1} (CH2 rocking) and 1280 cm^{-1} (CF2 stretching). Among these peaks, the F(β) values of the representative 763 cm^{-1} α peak and 840 cm^{-1} representative β peak were calculated using [32, 33]:

$$F(\beta) = \frac{A_\beta}{\left(K_\beta/K_\alpha\right)A_\alpha + A_\beta}. \quad (1)$$

As the SWCNT content increased, the size of the β-phase peaks and the F(β) value of the fabricated PVDF/SWCNT decreased, and the standard deviation of the β-phase peaks of the samples increased over repeated experiments, as shown in Fig. 7. These results are attributed to the lowered charge repulsion force and some interference due to the presence of SWCNT for the conversion of PVDF from the α to β phases during electrospinning. In addition, the increase in the standard deviation of the peak according to the repeated experiment in Fig. 7c is due to the electrospinning behavior becoming unstable because the current fluctuated significantly as the SWCNT content increased. Accordingly, as the SWCNT content increased, the peak standard deviation of the prepared web increased because of the unstable electrospinning behavior.

Conclusion

The effects of changes in the solution properties, spinning behaviors, and web structure at different SWCNT contents on the fabrication of PVDF/SWCNT webs through electrospinning were confirmed. The shear viscosity,

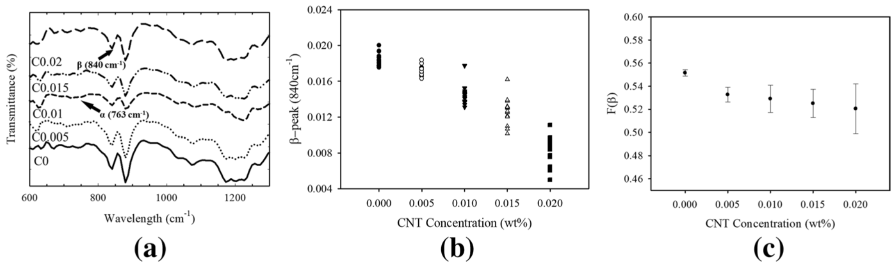

Fig. 7 **a** FT-IR spectra of PVDF/SWCNT webs. **b** FT-IR peak. **c** β-phase content

electrical conductivity, and surface tension increased with the SWCNT content. The increased shear viscosity and electrical conductivity at higher SWCNT content led to a decrease in the area and angle of the jet, as identified by analyzing the images captured using a CCD camera. The decrease in the jet angle caused a decrease in the elongation of the fibers formed during electrospinning and an increase in the fiber diameter, as confirmed through structural analysis. In addition, FT-IR analysis results confirmed the effects of SWCNT addition on nanoweb crystal formation. The β phase decreased with the addition of SWCNT, which hindered crystal formation during electrospinning. Changes in the solution properties have a significant effect on the electrospinning behavior and structural changes of the resulting fibers. As the spinning behavior changed with increasing SWCNT content, the fiber diameter increased, and the PVDF beta phase content and collection area tended to decrease. These results are expected to be useful for controlling the diameter, collection area, and various properties of the electrospinning process of composite materials of various polymers, conductive materials, and PVDF. In addition, electrospinning is generally referred to as a method for fabricating fibers or nonwoven materials, and research on electrospinning has tended to focus on changing the performance of the fabricated application. This study, unlike these, did not focus on the applications fabricated by electrospinning; rather, it focused on intensive analysis of electrospinning behavior to investigate the effect on the properties of fabricated fibers and nonwovens. Based on this, we believe that further analysis and research can be conducted by investigating the effect of electrospinning behavior when manufacturing and evaluating applications.

Acknowledgements This work was supported by the Technology Innovation Program (or Industrial Strategic Technology Development Program) (20017666, Development of technology to manufacture nanofiber separators for future automobiles using thermoplastic materials), funded by the Ministry of Trade, Industry & Energy (MOTIE, Korea).

Declarations

Conflict of interest The authors declare no conflict of interest.

References

1. Saxena P, Shukla P (2021) A comprehensive review on fundamental properties and applications of poly(vinylidene fluoride) (PVDF). Adv Compos Hybrid Mater 4:8–26. https://doi.org/10.1007/s42114-021-00217-0
2. Sukumaran S, Chatbouri S, Rouxel D et al (2020) Recent advances in flexible PVDF based piezoelectric polymer devices for energy harvesting applications. J Intell Mater Syst Struct 32:746–780. https://doi.org/10.1177/1045389x20966058
3. Pornea AM, Puguan JMC, Deonikar VG et al (2020) Fabrication of multifunctional wax infused porous PVDF film with switchable temperature response surface and anti corrosion property. J Ind Eng Chem 82:211–219. https://doi.org/10.1016/j.jiec.2019.10.015
4. Barrau S, Ferri A, Da Costa A et al (2018) Nanoscale investigations of alpha- and gamma-crystal phases in PVDF-based nanocomposites. ACS Appl Mater Interfaces 10:13092–13099. https://doi.org/10.1021/acsami.8b02172

5. Pickford T, Gu X, Heeley EL et al (2019) Effects of an ionic liquid and processing conditions on the β-polymorph crystal formation in poly(vinylidene fluoride). CrystEngComm 21:5418–5428. https://doi.org/10.1039/c9ce01051c
6. Bairagi S, Ali SW (2019) A unique piezoelectric nanogenerator composed of melt-spun PVDF/KNN nanorod-based nanocomposite fibre. Eur Polym J 116:554–561. https://doi.org/10.1016/j.eurpolymj.2019.04.043
7. Luo M, Luo H, Axinte D et al (2018) A wireless instrumented milling cutter system with embedded PVDF sensors. Mech Syst Signal Process 110:556–568. https://doi.org/10.1016/j.ymssp.2018.03.040
8. Kalimuldina G, Turdakyn N, Abay I et al (2020) A review of piezoelectric PVDF film by electrospinning and its applications. Sensors (Basel). https://doi.org/10.3390/s20185214
9. Sanyal A, Sinha-Ray S (2021) Ultrafine PVDF nanofibers for filtration of air-borne particulate matters: a comprehensive review. Polymers (Basel). https://doi.org/10.3390/polym13111864
10. Al Rai A, Stojanovska E, Fidan G et al (2020) Structure and performance of electroblown PVDF-based nanofibrous electret filters. Polym Eng Sci 60:1186–1193. https://doi.org/10.1002/pen.25372
11. Luiso S, Henry JJ, Pourdeyhimi B et al (2021) Meltblown polyvinylidene difluoride as a Li-ion battery separator. ACS Appl Polym Mater 3:3038–3048. https://doi.org/10.1021/acsapm.1c00221
12. Valverde A, Gonçalves R, Silva MM et al (2020) Metal–organic framework based PVDF separators for high rate cycling lithium-ion batteries. ACS Appl Energy Mater 3:11907–11919. https://doi.org/10.1021/acsaem.0c02044
13. Hall D (2001) Review nonlinearity in piezoelectric ceramics. J Mater Sci 36:4575–4601. https://doi.org/10.1023/A:1017959111402
14. Lim J, Kim HS (2021) Effects of SWCNT/PVDF composite web behavior on acoustic piezoelectric property. Sens Actuators A Phys. https://doi.org/10.1016/j.sna.2021.112840
15. Lee C, Tarbutton JA (2019) Polyvinylidene fluoride (PVDF) direct printing for sensors and actuators. Int J Adv Manuf Technol 104:3155–3162. https://doi.org/10.1007/s00170-019-04275-z
16. Ghosal K, Agatemor C, Špitálsky Z et al (2019) Electrospinning tissue engineering and wound dressing scaffolds from polymer-titanium dioxide nanocomposites. Chem Eng J 358:1262–1278. https://doi.org/10.1016/J.CEJ.2018.10.117
17. Altinkok C, Acik G, Daglar O et al (2022) A facile approach for the fabrication of antibacterial nanocomposites: a case study for AgNWs/poly(1,4-cyclohexanedimethylene acetylene dicarboxylate) composite networks by aza-Michael addition. Eur Polym J. https://doi.org/10.1016/j.eurpolymj.2022.111130
18. Armentano I, Puglia D, Luzi F et al (2018) Nanocomposites based on biodegradable polymers. Materials (Basel). https://doi.org/10.3390/ma11050795
19. Son WK, Youk JH, Park WH (2006) Antimicrobial cellulose acetate nanofibers containing silver nanoparticles. Carbohydr Polym 65:430–434. https://doi.org/10.1016/j.carbpol.2006.01.037
20. Choudhury A (2009) Polyaniline/silver nanocomposites: dielectric properties and ethanol vapour sensitivity. Sens Actuators B Chem 138:318–325. https://doi.org/10.1016/j.snb.2009.01.019
21. Acik G (2021) Fabrication of polypropylene fibers possessing quaternized ammonium salt based on the combination of CuAAC click chemistry and electrospinning. React Funct Polym. https://doi.org/10.1016/j.reactfunctpolym.2021.105035
22. Ruan L, Yao X, Chang Y et al (2018) Properties and applications of the beta phase poly(vinylidene fluoride). Polymers (Basel). https://doi.org/10.3390/polym10030228
23. Gade H, Nikam S, Chase GG et al (2021) Effect of electrospinning conditions on β-phase and surface charge potential of PVDF fibers. Polymer. https://doi.org/10.1016/j.polymer.2021.123902
24. Zaarour B, Zhu L, Huang C et al (2019) Enhanced piezoelectric properties of randomly oriented and aligned electrospun PVDF fibers by regulating the surface morphology. J Appl Polym Sci. https://doi.org/10.1002/app.47049
25. Faraz M, Singh HH, Khare N (2022) A progressive strategy for harvesting mechanical energy using flexible PVDF-rGO-MoS2 nanocomposites film-based piezoelectric nanogenerator. J Alloys Compd. https://doi.org/10.1016/j.jallcom.2021.161840
26. Eun JH, Sung SM, Kim MS et al (2021) Effect of MWCNT content on the mechanical and piezoelectric properties of PVDF nanofibers. Mater Des. https://doi.org/10.1016/j.matdes.2021.109785
27. Anand S, Pauline S (2021) Electromagnetic interference shielding properties of BaCo2Fe16O27 nanoplatelets and RGO reinforced PVDF polymer composite flexible films. Adv Mater Interfaces 8:2001810. https://doi.org/10.1002/admi.202001810

28. Qi S, Craig D (2016) Recent developments in micro- and nanofabrication techniques for the preparation of amorphous pharmaceutical dosage forms. Adv Drug Deliv Rev 100:67–84. https://doi.org/10.1016/j.addr.2016.01.003
29. Yousefzade O, Katsarava R, Puiggali J (2020) Biomimetic hybrid systems for tissue engineering. Biomimetics (Basel). https://doi.org/10.3390/biomimetics5040049
30. Jang S, Song S, Lim JH et al (2020) Application of various metal–organic frameworks (MOFs) as catalysts for air and water pollution environmental remediation. Catalysts. https://doi.org/10.3390/catal10020195
31. Choi S, Kim HR, Jeong YK et al (2018) Mechanism of electrospinning for poly(amic acid)/polyacrylonitrile fiber fabrication. J Macromol Sci Part B 57:222–230. https://doi.org/10.1080/00222348.2018.1441221
32. Sorayani Bafqi MS, Bagherzadeh R, Latifi M (2015) Fabrication of composite PVDF-ZnO nanofiber mats by electrospinning for energy scavenging application with enhanced efficiency. J Polym Res. https://doi.org/10.1007/s10965-015-0765-8
33. Sharma M, Madras G, Bose S (2014) Process induced electroactive beta-polymorph in PVDF: effect on dielectric and ferroelectric properties. Phys Chem Chem Phys 16:14792–14799. https://doi.org/10.1039/c4cp01004c